Hindawi
Journal of Sensors
Volume 2021, Article ID 8888187, 13 pages
https://doi.org/10.1155/2021/8888187

Research Article

High-Precision Complementary Metamaterial Sensor Using Slotted Microstrip Transmission Line

Abdul Samad, Wei Dong Hu, Waseem Shahzad, Leo. P. Ligthart, and Hamid Raza

School of Information and Electronics, Beijing Institute of Technology (BIT), Beijing 100081, China

Correspondence should be addressed to Wei Dong Hu; hoowind@bit.edu.cn

Received 3 March 2020; Revised 23 October 2020; Accepted 2 July 2021; Published 3 August 2021

Academic Editor: Francesco Dell'Olio

Metamaterial-based microwave sensor having novel and compact structure of the resonators and the slotted microstrip transmission line is proposed for highly precise measurement of dielectric properties of the materials under test (MUTs). The proposed sensor is designed and simulated on Rogers' substrate RO4003C by using the ANSYS HFSS software. A single and accumulative notch depth of -44.29 dB in the transmission coefficient (S_{21}) is achieved at the resonant frequency of 5.15 GHz. The negative constitutive parameters (permittivity and permeability) are extracted from the *S*-parameters which are the basic property of metamaterials or left handed materials (LHMs). The proposed sensor is fabricated and measured through the PNA-X (N5247A). The sensitivity analysis is performed by placing various standard dielectric materials onto the sensor and measuring the shift in the resonant frequencies of the MUTs. A parabolic equation of the proposed sensor is formulated to approximate the resonant frequency and the relative permittivity of the MUTs. A very strong agreement among the simulated, measured, and calculated results is found which reveals that the proposed sensor is a highly precise sensor for the characterization of dielectric properties of the MUTs. Error analysis is performed to determine the accuracy of the proposed sensor. A very small percentage of error (0.81%) and a very low standard deviation are obtained which indicate high accuracy of the proposed sensor.

1. Introduction

Since the invention of metamaterials or left handed materials (LHMs), having unnatural and unique properties of the negative constitutive parameters [1, 2], the researchers and industries have produced numerous improved devices for the broad applications in the frequency range from RF to THz. Metamaterials are classified into two broad groups in which one is the split ring resonators (SRRs), introduced by Pendry et al., [3] and other is the complementary SRR (CSRR), introduced by Falcone et al. [4]. They have been used in the miniaturization of oscillators [5, 6], microwave filters [7, 8], microwave sensors [9–12], and communication antennas [13–16].

The microwave sensors based on the SRRs [17–21] and CSRRs [22–27] have widely been used in various applications. The SRR structures are etched on the top plane of the sensor near the microstrip line. They couple magnetically with the microstrip line. Owing to the small electric fringing fields, the sensors based on the SRR are less efficient for the characterization of large samples in the microwave frequency range. The CSRRs are suitable for the measurement of large samples. The CSRR is the negative image of the SRR and etched in the ground plane of the sensor. They couple electrically with the microstrip line. At resonance, the large electric fringing fields produce in the ground plane which has been used for the characterization of materials' thickness [28], loss tangent [29], healthcare [30], agriculture [31], organic tissues analysis [32], and environment [33].

The precise measurement of the dielectric properties is essential while characterizing the materials under test (MUTs). Permittivity is one of the important parameters to analyze the behavior of the materials. For the development of the sophisticated microwave devices, prior knowledge of the materials' permittivity is necessary. There are four types of approaches classified for the characterization of the MUTs including free space, transmission line, near field, and resonance based [34]. Among them, the resonance-based approach is implemented in the present work which is economical, efficient, and highly precise for the measurement

of dielectric properties of the MUTs. Particularly, the use of complementary metamaterial sensor for the measurement of dielectric properties of the MUTs is very convenient since the capacitance (and hence the resonant frequency) is very sensitive to the presence of the MUT onto the sensor. The variation of the sensing stimuli modifies the resonant properties of the sensor like notch frequency, Q-factor, and notch depth during the interaction [35]. On the basis of the measured data, dielectric properties of various MUTs can be estimated.

In literature, the metamaterial sensors based on multiresonators on a single PCB board have been reported [21, 32, 36–38]. They provide multiresonant frequency bands instead of a single resonant frequency band. In [36, 37], two resonators have been etched on a single board that provide two resonant frequency bands instead of a single resonant frequency band. Similarly, in [38], three and four resonators have been etched on a single board that provide three and four resonant frequency bands, respectively, rather a single resonant frequency band. A single and sharp resonant frequency band with deep notch in the transmission coefficient (S_{21}) has a significant role for the precise measurement of dielectric properties of the MUTs [39]. A metamaterial sensor based on an array of multiresonators that provides a single resonant frequency band is required to be developed for the precise measurement of dielectric properties of the MUTs. In the present work, a highly accurate metamaterial sensor based on the slotted microstrip line and four compact resonators is proposed. An array of four symmetrical resonators is etched in the ground plane of the sensor keeping in view the geometrical and parametrical measures for achieving a single and accumulative notch in the transmission coefficient (S_{21}). The equivalent circuit model of the proposed sensor is developed that describes the overall behavior of the sensor.

2. Design and Parametric Analysis

The proposed sensor is designed on the substrate RO4003C on using the ANSYS HFSS. The thickness of the substrate is optimized to 1 mm, whereas the length and width of the substrate are optimized to 35 mm and 15 mm, respectively. Both the layers (top and bottom) of the substrate are coated with copper having thickness of 0.017 mm. The top copper layer of the substrate consists of a slotted microstrip transmission line. The width of the line is optimized to 2.2 mm to achieve the characteristic impedance of 50 Ω using the expressions of the microstrip transmission line [40]. An array of four symmetrical resonators is etched from the copper layer in the ground plane as shown in Figure 1. The dimensions of all the resonators are the same ($l = 5$, $w = 3$, $h = 0.017$). All the dimensions in this work are taken in the mm scale.

The slotted microstrip transmission line as shown in Figure 1(a) is introduced in this work to enhance the sensitivity of the proposed sensor. The slots in the microstrip line are used to increase the flux concentration which in turn increases the electric fringing field. The sensitivity of the sensor increases with the increase in the electric fringing fields. The dimensions of every slot are 5 mm, whereas the spacing among the pairs of slots 1 mm. The other dimensions of the design parameters of the microstrip line as shown in Figure 1(a) are ($a = b = 0.35$ mm) and ($c = d = e = 0.5$ mm). The effect of these microstrip line parameters is analyzed on the resonant characteristics of the proposed sensor on using the ANSYS HFSS. The parameters a and b represent the capacitive elements, whereas the parameters c, d, and e represent the inductive elements. By increasing a and b one by one, the effective capacitance of the sensor decreases which in turn increases the resonant frequency (f_r) of the sensor according to the equation (1). Contrarily, by increasing c, d, and e, copper area around the slots increases which in turn decreases the inductance of the sensor. The decrease in the inductance, the resonant frequency (f_r) of the sensor increases. Graphical representation of the effects of the design parameters of the microstrip line on the resonant characteristics of the sensor is shown in Figure 2.

The resonant characteristics of the sensor can also be controlled by varying the design parameters of the resonators (m, n, o, p,g) as shown in Figure 1(c). The dimensions of the design parameters of the resonators are ($m = n = o = p = g =$ 0.3 mm). The parameters m and n designate the outer and inner rectangles, respectively, which represent the capacitive element while the parameters o and g designate the thickness between the rectangles and slits, respectively, which represent the inductive element of the sensor. By increasing the parameters m and n one by one, the effective capacitance decreases which in turn increases the resonant frequency (f_r) of the sensor.

However, increasing the parameter p, the copper area of the inner ring of the resonator reduces. Keeping in view the cylindrical geometry, inner radius of the cylinder decreases which in turn increases the overall inductance of the sensor. As an increase in the inductance, the resonant frequency (f_r) of the sensor decreases. Graphical representation of the effects of the design parameters of the resonators on the resonant characteristics is shown in Figure 3.

Keeping in view the parametrical and geometrical measures, the position of each resonator in an array is taken wisely to maintain the coupling with the neighboring resonators and keep the board size quite compact. If the spacing among the resonators is brought close to one another (less than 1 mm), the coupling tends to degrade the performance of the sensor, specifically the sensitivity at small perturbations. If the spacing among the resonators is increased enough, the cross coupling effect weakens, and more notches appear in the transmission coefficient. So, the optimized spacing among the resonators is concluded to 1 mm for achieving the desired response in terms of a single resonant frequency band from the sensor after numerous iterative simulations.

The overall behavior of the proposed sensor can be analyzed by its lumped element equivalent circuit model as shown in Figure 4. The equivalent circuit model is developed on using the NI Multisim software. The resonance structure of the sensor consists of two parts; first is the top part of the substrate which is composed of the slotted microstrip line with a coupling capacitance represented by the symbol C_c. The second part is the MUT layer, in the ground plane of the substrate, which has a variable capacitance represented

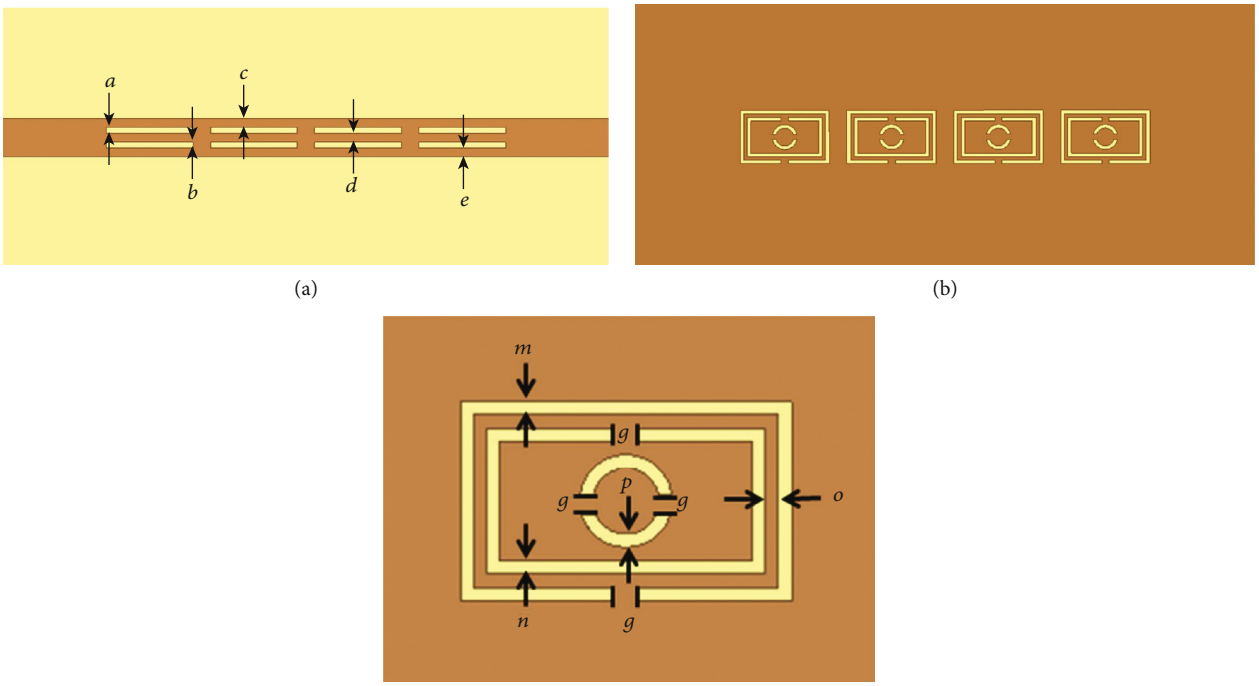

Figure 1: Layout of the proposed sensor: (a) The slotted microstrip line on the top plane, (b) an array of four resonators etched in the ground plane, and (c) dimensions of the resonator.

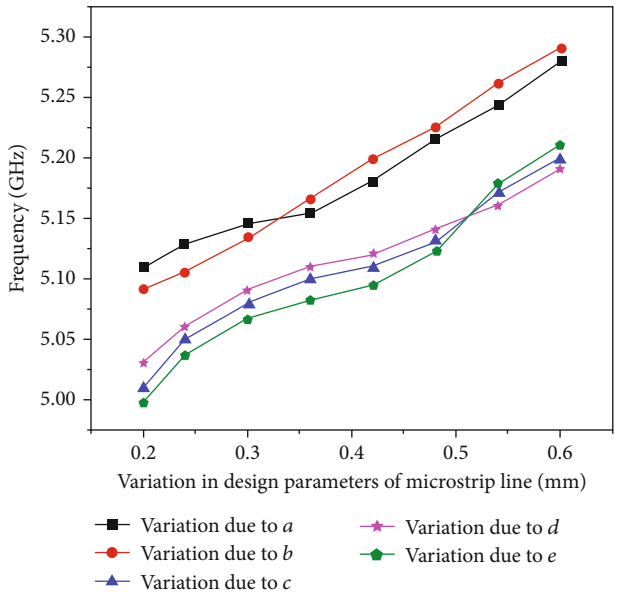

Figure 2: Effect of the design parameters of the microstrip line on the resonant characteristics of the sensor.

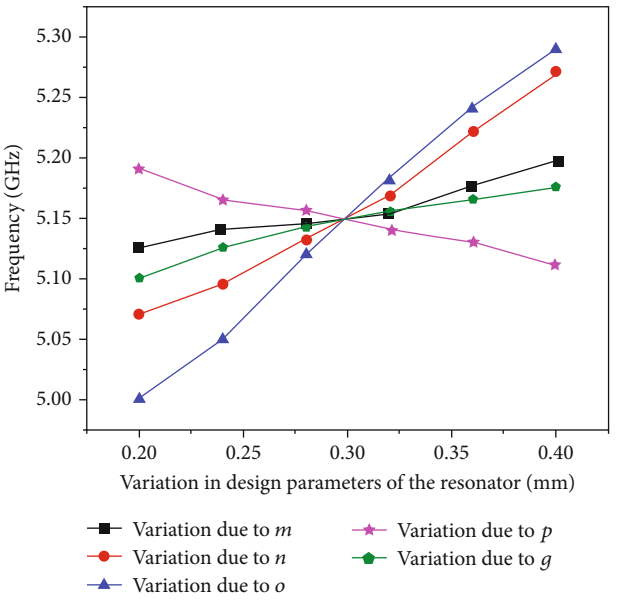

Figure 3: Effect of the design parameters of the resonators on the resonant characteristics of the sensor.

by the symbol C_r. These two parts provide with two shunt capacitance values that form the total capacitance of the sensor. The symbols L_r and R_r represent the inductance and resistance of the unit cell, respectively. The resistance (R_r) accounting for the losses in the unit cell, whereas the parallel combination of four inductances labeled with the symbol L_s represents the line inductance. By optimizing the design parameters of the slotted microstrip line and the resonators, performance of the sensor can be controlled effectively. The optimized expression for the proposed resonator can be modelled by an RLC circuit whose resonant frequency (f_r) is given by [41]

$$f_{\mathrm{r}} = \frac{1}{2\pi\sqrt{L_r(C_c + C_r)}}. \quad (1)$$

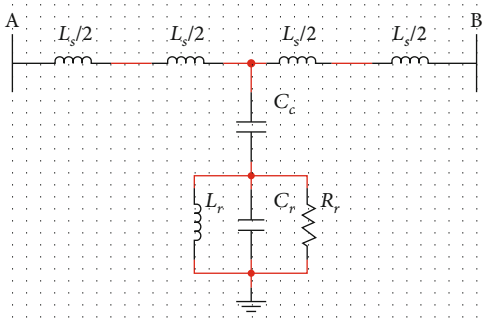

Figure 4: Lumped element equivalent circuit for the basic cell of the resonator loaded microstrip line.

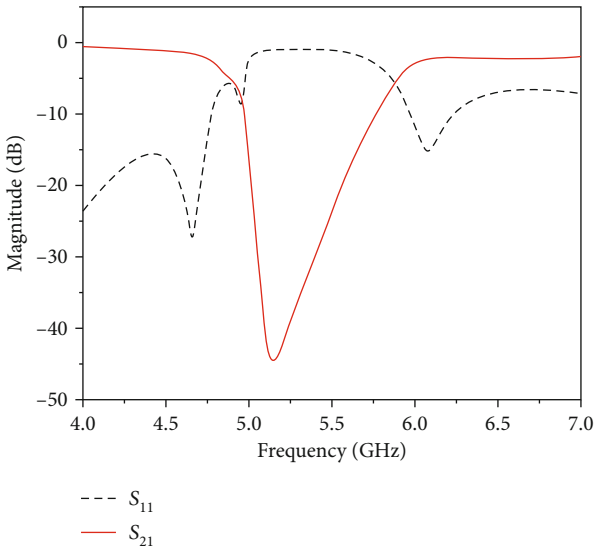

Figure 5: Magnitudes of S-parameters of the proposed sensor.

The resonant frequency (f_r) of the resonators couple with the microstrip line is the function of three parameters (L_r, C_r, and C_c). With the change in the inductance and capacitance due to the interaction with the MUTs, the resonant frequency of the sensor changes accordingly.

2.1. Simulations and Performance Analysis. The proposed sensor is designed and simulated on using the ANSYS HFSS. The magnitudes of S-parameters (reflection (S_{11}) and transmission (S_{21}) coefficients) of the proposed sensor are shown in Figure 5. An accumulative notch depth of -44.29 dB in the transmission coefficient (S_{21}) is achieved at the resonant frequency of 5.15 GHz. Four symmetrical resonators are etched in the ground plane in an array after numerous iterative simulations so that with the increase in the number of resonators, the notch depth in the transmission coefficient also increases but the resonant frequency remains the same. There are four notches at -22.18 dB, -29.72 dB, -37.45 dB, and -44.29 dB achieved with one, two, three, and four resonators, respectively, which have been merged into a single graph by using the OriginPro 8 software, which are shown in Figure 6 and numerically described in Table 1.

The constitutive effective parameters (permittivity (ε) and permeability (μ)) of the proposed metamaterial sensor

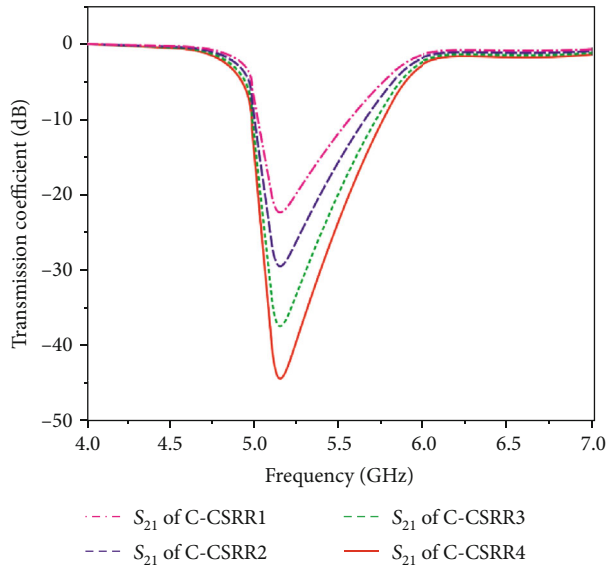

Figure 6: Response of the resonators in terms of notch depth and resonant frequency.

Table 1: Effect of each resonator on the resonant frequency and notch depth.

Number of resonators	Resonance (GHz)	Notch depth (dB)
One	5.15	-22.18
Two	5.15	-29.72
Three	5.15	-37.45
Four	5.15	-44.29

are retrieved from the S-parameter data. By properly coupling the CSRR structure to a host microstrip line, the structure with the negative constitutive parameters can be obtained. In order to obtain a left-handed transmission line based on the CSRR structures, an effective negative valued permeability can be achieved by periodically etching the capacitive gaps in the conductor strip at periodic positions [17]. The graphs of the effective permittivity and permeability are shown in Figure 7. Both the effective permittivity and permeability are negative at vicinity of the resonant frequency. The permittivity is negative from 5.125 GHz to 5.167 GHz, whereas the permeability is negative from 5.22 GHz to 5.73 GHz, which is the basic property of metamaterials/LHMs.

The effective permittivity and permeability of the metamaterial sensor can be retrieved from its transmission (S_{21}) and reflection (S_{11}) coefficients using the following expressions [42].

$$S11 = \frac{R_{01}\left(1\text{-}e^{i2nkod}\right)}{1\text{-}R_{01}^2 e^{i2nkod}}, \tag{2}$$

$$S21 = \frac{\left(1\text{-}R_{01}^2\right)e^{inkod}}{1\text{-}R_{01}^2 e^{i2nkod}}. \tag{3}$$

Since $R_{01} = z - 1/z + 1$.

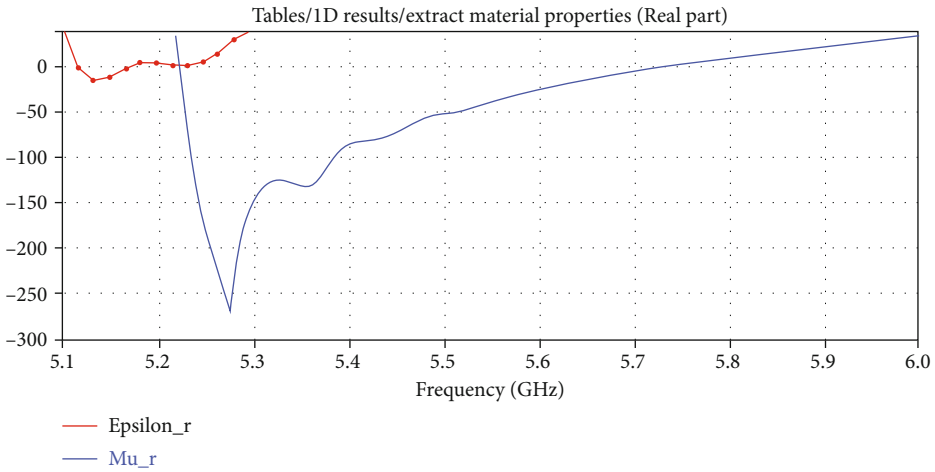

Figure 7: Extracted plots of the effective permittivity and permeability of the proposed sensor.

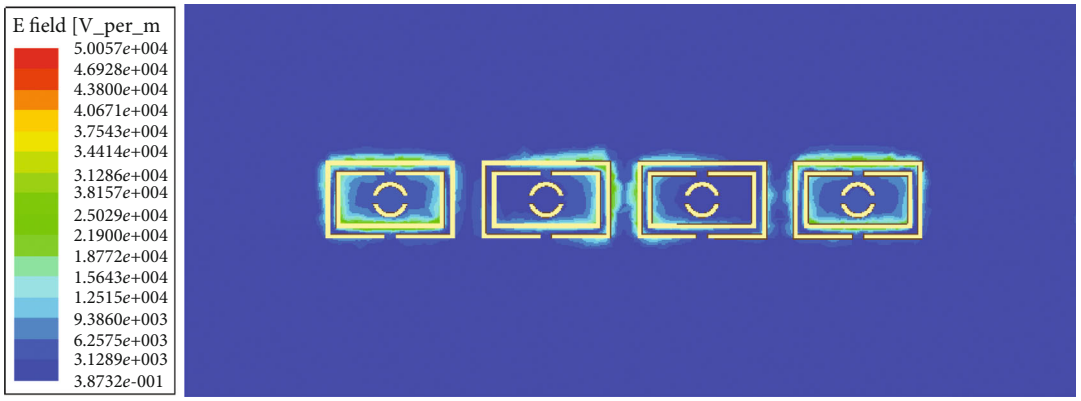

Figure 8: The electric field concentration of the proposed sensor.

n is the refractive index, z is the impedance, k_0 is the wave number of the incident wave in free space, d is the thickness of material/slab, and m is an integer related to the branch index. The refractive index (n) and the impedance (z) are obtained by inverting the equations (2) and (3), yielding

$$z = \pm\left\{\sqrt{\frac{(1+S_{11})^2 - S_{21}^2}{(1-S_{11})^2 - S_{21}^2}}\right\}, \tag{4}$$

$$Q = e^{inkod} = \frac{S_{21}}{1 - S_{11}(z - 1/z + 1)}, \tag{5}$$

$$n = \frac{1}{k_o d}[\{\mathrm{Im}\,[\ln(Q)] + 2m\pi\} - i.\mathrm{Re}\,[\ln(Q)]]. \tag{6}$$

Both the effective permittivity (ε) and permeability (μ) are associated with the refractive index (n) and the impedance (z) as

$$\varepsilon = \frac{n}{z}, \tag{7}$$

$$\mu = nz. \tag{8}$$

The electric and magnetic field distributions around the resonators are investigated for efficient characterization of the MUTs. Concentrations of the electric and magnetic fields around every resonator are shown in Figures 8 and 9, respectively. The maximum electric field concentration around the proposed resonators is 5×10^4 V/m, and the magnetic field concentration is 1.91×10^2 A/m. When a MUT is placed onto the resonators for the characterization, then the electric field gets perturbed. This perturbation of electric field leads to change in the resonant frequency of the sensor. To map the change in the resonant frequencies with the permittivity of the MUT, a numerical model for the proposed sensor is developed to approximate the permittivity of the MUTs.

2.2. Numerical Simulations. From the theory of perturbation, when a MUT is placed onto the sensor, it interacts with the electric and magnetic fields of the sensor and perturbs the field distributions. Consequently, phenomena of shift in the resonant frequency occur. The relation between the resonant frequency of a microwave sensor and the dielectric properties of the MUTs can be described numerically as [41]

$$\frac{\Delta fr}{fr} = \frac{\int_v (\Delta\varepsilon E_1 . E_0 + \Delta\mu H_1 . H_0)dv}{\int_v (\varepsilon_0 |E_0|^2 + \mu 0 |H_0|^2)dv}. \tag{9}$$

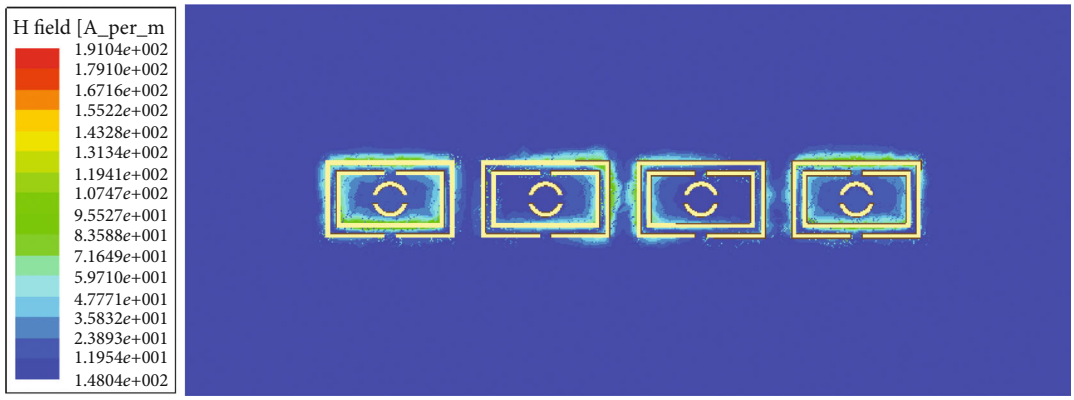

Figure 9: The magnetic field concentration of the proposed sensor.

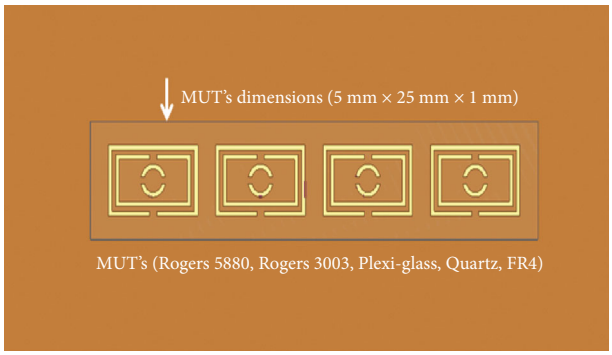

Figure 10: Position of the MUTs in the ground plane of the proposed sensor.

Here,Δf_r is the shift in the resonant frequency (f_r) due to the interaction with the MUTs. ε_0 and μ_0 are the permittivity and permeability of the free space while $\Delta\varepsilon$ and $\Delta\mu$ are the change in the permittivity and permeability, respectively. E_0 and H_0 are the electric and magnetic fields before the interaction with the MUTs, whereas E_1 and H_1 are the perturbed fields and v is the perturbed volume. If the intensity of the magnetic field is higher than that of the electric field, the phenomenon of the shift in the resonant frequency occurs due to the permeability of the MUT. Contrarily, if the intensity of the electric field is higher, the shift in the resonant frequency occurs due to the permittivity of the MUT. In the present work, the intensity of the electric field is higher than that of the magnetic field; hence, the phenomenon of the shift in the resonant frequency occurs due to the interaction with the permittivity of the MUT.

The sensitivity analysis is performed using the proposed sensor through the ANSYS HFSS. The shift in the resonant frequency of the proposed sensor is measured under both the loaded and unloaded conditions. The standard MUTs including Rogers 5880, Rogers 3003, Plexi-glass, Quartz, and FR4 are used in the present work for the sensitivity analysis. These MUTs with the same dimensions (5 mm× 25 mm×1 mm) are placed one by one onto the array of resonators in the ground plane without air gap, as shown in Figure 10 and measuring the shift in the resonant frequency of the sensor due to the interaction with these MUTs, as shown in Figure 11. By increasing the permittivity of the

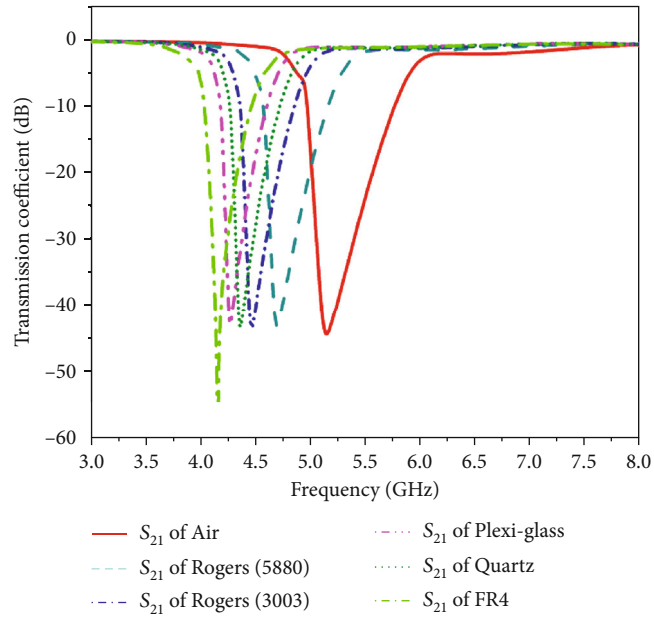

Figure 11: Shift in the resonant frequency of the proposed sensor due to the interaction with the MUTs.

Table 2: Shift in the resonant frequency of the sensor due to the interaction with the MUTs.

MUTs	Permittivity of MUTs ($\varepsilon_{r,\ MUT}$)	Resonance ($f_{r,\ MUT}$) (GHz)
Air	1	5.15
Rogers 5880	2.2	4.70
Rogers 3003	3	4.47
Plexi-glass	3.4	4.36
Quartz	3.75	4.27
FR4	4.3	4.16

MUT, the resonant frequency of the sensor decreases accordingly. The shift in the resonant frequency corresponding to every value of the permittivity of the MUTs is recorded and tabulated in Table 2.

Basically, when a MUT is placed onto the resonator, it perturbs the field distributions during the interaction.

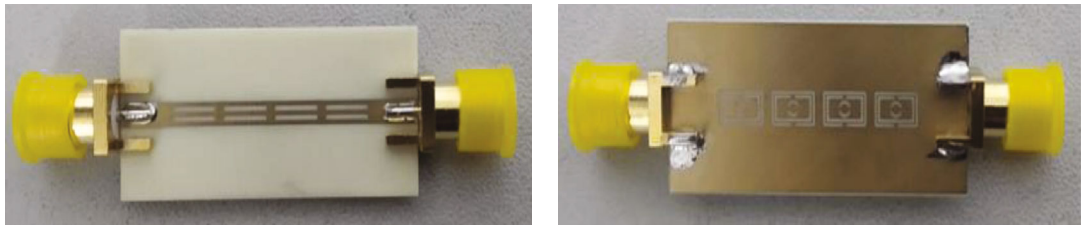

(a) (b)

Figure 12: Fabricated sensor on RO4003C substrate. (a) The top plane with the microstrip transmission line. (b) The bottom plane with an array of four resonators.

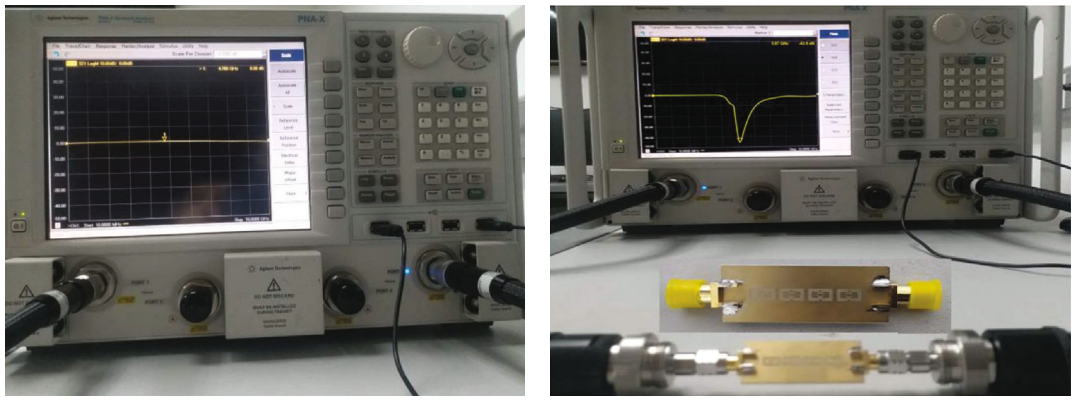

(a) (b)

Figure 13: Measurement through PNA-X (N5247A); (a) SOLT calibration and (b) transmission coefficient (S_{21}) of the fabricated sensor (unloaded condition).

Consequently, the capacitance of the sensor increases which in turn decreases the resonant frequency as discussed in equation (1).

2.3. Fabrication and Measurement. The proposed sensor is fabricated on the substrate RO4003C by using the standard photolithography procedures. The dielectric constant of the substrate is 3.55, whereas the loss tangent is 0.0027. The thickness of the substrate is optimized to 1 mm. Both the planes (top and bottom) of the substrate are coated with the copper layer having thickness of 0.017 mm. The top copper plane of the substrate consists of a slotted microstrip transmission line, whereas an array of four resonators is etched in the ground plane as shown in Figure 12. The PNA-X (N5247A) is used to measure the response of the fabricated sensor. The short open load through (SOLT) calibration is performed using the Agilent electronic calibration kit as shown in Figure 13(a). A pair of 50 Ω SMA connectors is used to connect the fabricated sensor with the PNA-X. The response of the fabricated sensor in terms of the resonant frequency and notch depth in the transmission coefficient (S_{21}) is measured without placing the MUT (unloaded condition). The notch depth of -43.9 dB in the transmission coefficient is measured at the resonant frequency of 5.07 GHz as shown in Figure 13(b). The comparison between the simulated and measured response of the proposed sensor is shown in Figure 14, which depicts a very strong agreement between them.

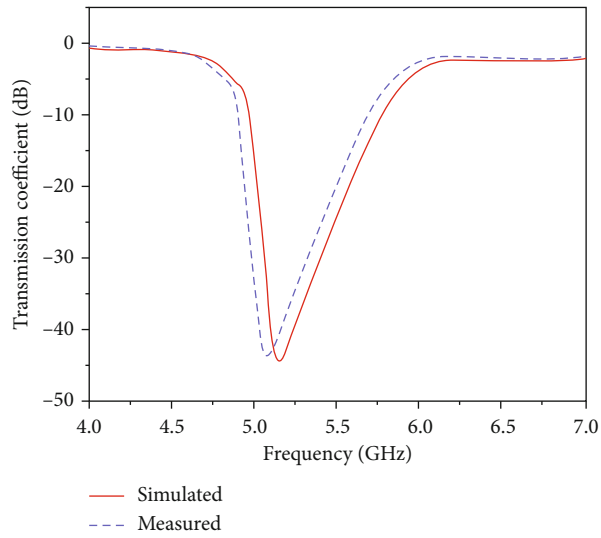

Figure 14: Comparison between simulated and measured response of the proposed sensor.

The sensitivity analysis is performed using the fabricated sensor through the PNA-X by placing the standard MUTs including Rogers 5880, Rogers 3003, Plexi-glass, Quartz, and FR4 one by one without air gap as shown in Figure 15(a) and measuring the shift in the resonant frequency of the sensor. The measured response of the fabricated sensor is shown

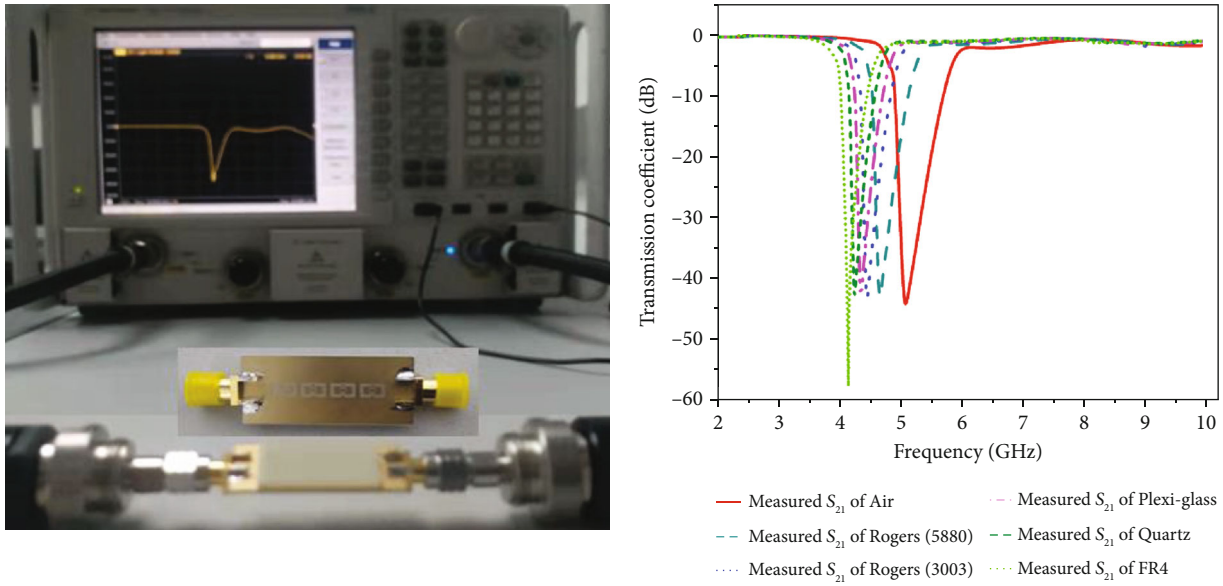

(a) (b)

Figure 15: Measured results of the proposed sensor through PNA-X. (a) Placement of MUTs onto the resonators in the ground plane. (b) Shift in the resonant frequency due to the interaction with the standard MUTs.

Table 3: Comparison of simulated and measured response of the proposed sensor and error analysis.

MUTs	Permittivity ($\varepsilon_{r,\mathrm{MUT}}$)	Tan δ	Simulated freq. (GHz)	Measured freq. (GHz)	% error	STD
Air	1	0	5.15	5.07	1.55	0.001
Rogers 5880	2.2	0.0009	4.70	4.66	0.85	0.004
Rogers 3003	3	0.0013	4.47	4.43	0.89	0.007
Plexi-glass	3.4	0.0010	4.36	4.33	0.68	0.009
Quartz	3.75	0	4.27	4.25	0.46	0.012
FR4	4.3	0.02	4.16	4.14	0.48	0.017

in Figure 15(b). All the MUTs are measured four times alternatively to observe the behavior of the fabricated sensor. All the times, the measured results are almost same because the MUTs are placed onto the sensor without air gap, and every measurement is performed at the room temperature. A comparison between the simulated and measured response in terms of shift in the resonant frequency of the sensor is presented in Table 3. A very small difference in the measured and simulated response reveals a strong agreement between them. Error analysis between the simulated and measured results is carried out, whereas the standard deviation (STD) of the measured results is calculated to determine the accuracy of the proposed sensor, which is also tabulated in Table 3. A very small percentage of error and a low standard deviation is obtained which indicate high accuracy of the proposed sensor. An error bar graph with the standard deviation is shown in Figure 16, which illustrates a very low standard deviation and a strong agreement between the simulated and measured response of the proposed sensor.

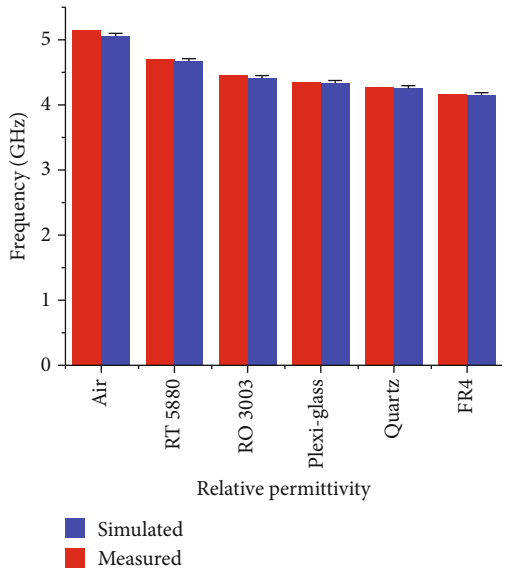

Figure 16: Error bar graph and standard deviation of the measured response of the proposed sensor.

2.4. Equation Formulation. The parabolic equation for the proposed sensor with fitting parameters is formulated for the approximation of the relative permittivity of the materials under test. The parabolic equation is fairly reliable to

Table 4: Comparison of measured and calculated response in terms of resonant frequencies and error analysis.

MUTs	Permittivity ($\varepsilon_{r,\mathrm{MUT}}$)	Measured ($f_{r,\mathrm{MUT}}$) (GHz)	Calculated ($f_{r,\mathrm{MUT}}$) (GHz)	% error
Air	1	5.07	5.07	0.00
Rogers 5880	2.2	4.66	4.658	0.049
Rogers 3003	3	4.43	4.432	0.045
Plexi-glass	3.4	4.33	4.329	0.023
Quartz	3.75	4.25	4.249	0.023
FR4	4.3	4.14	4.138	0.048

Table 5: Comparison of the real and calculated response in terms of relative permittivity and error analysis.

MUTs	Measured ($f_{r,\mathrm{MUT}}$) (GHz)	Real permittivity	Calculated permittivity	% error
Air	5.07	1	1.002	0.19
Rogers 5880	4.66	2.2	2.196	0.18
Rogers 3003	4.43	3	3.002	0.07
Plexi-glass	4.33	3.4	3.402	0.06
Quartz	4.25	3.75	3.752	0.05
FR4	4.14	4.3	4.295	0.12

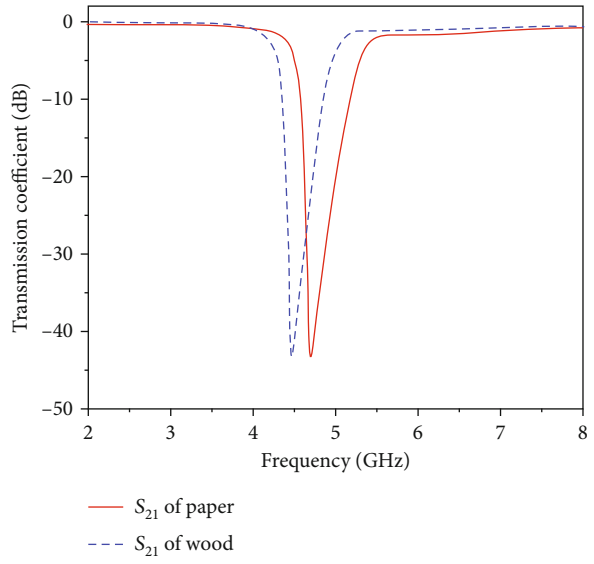

Figure 17: Measured responses of wood and paper through PNA-X.

approximate the relative permittivity of the materials ranging up to 10. The parabolic equation can be expressed as [43]

$$f_{r,\mathrm{MUT}} = A1 + A2(\varepsilon_{r,\mathrm{MUT}}) + A3(\varepsilon_{r,\mathrm{MUT}})^2. \quad (10)$$

Table 6: Comparison of real and calculated values of the effective permittivity of irregular MUTs.

MUTs	Measured ($f_{r,\mathrm{MUT}}$) (GHz)	Real permittivity	Calculated permittivity
Air	5.07	1	1.002
Paper	4.6	2.3~3.5	2.39
Wood	4.51	2.5~5.2	2.71

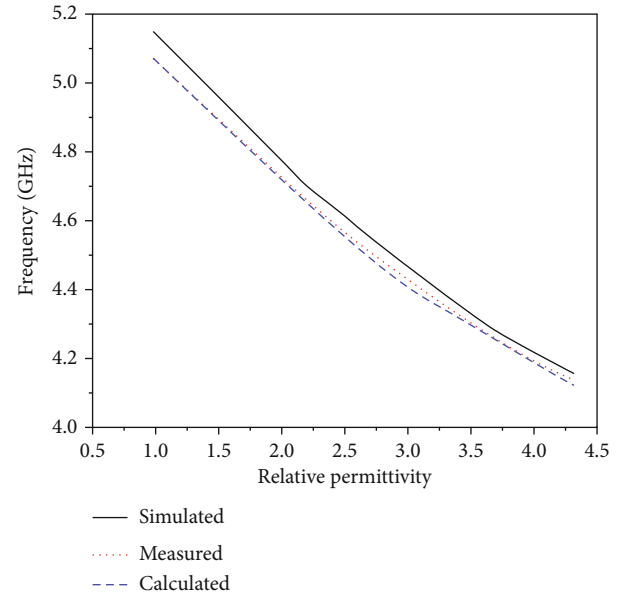

Figure 18: Graphical representation of the simulated, measured, and calculated resonant frequency.

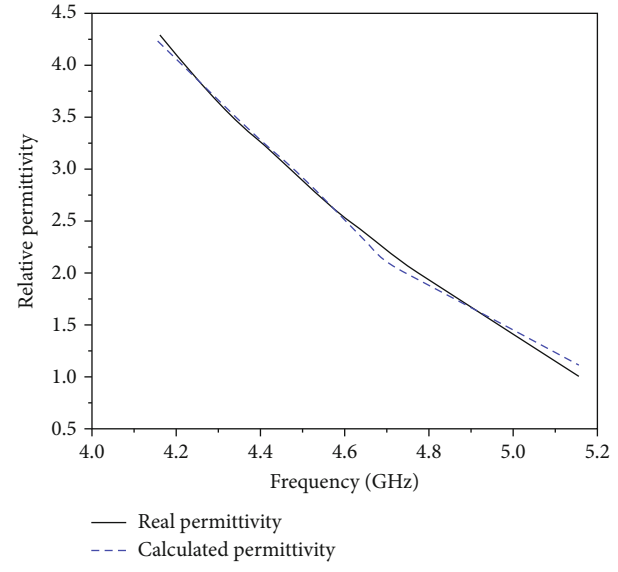

Figure 19: Graphical representation of the real and calculated permittivity of the MUTs.

Here $f_{r,\mathrm{MUT}}$ and $\varepsilon_{r,\mathrm{MUT}}$ are the resonant frequency and the relative permittivity of the MUT, respectively. A_1, A_2, and A_3 are the constants of polynomial. In this analysis, air

Table 7: Performance analysis between the proposed sensor and reported sensors in literature.

References	Sensor type	Permittivity range	Resonance (GHz)	Notch depth (dB)	% error (mean value)
[44]	SRR, rectangular	≈ 6.7	2.74	-13.24	4.62
[45]	SRR, rectangular	≈ 5.8	2.45	-13.87	2.84
[27]	CSRR, square	≈ 10	2.7	-17.48	3.43
[22]	CSRR, circular	≈ 2.3	2.65	-20.8	2.28
[36]	CSRR, circular	≈ 4.2	2.3	-18.7	3.23
			5.5	-25.83	3.74
[38]	CSRR, circular	≈ 2.65	1.5	-20.01	1.69
			2.45	-24.8	2.05
			3.8	-19.1	2.12
[41]	CSRR, square	≈ 4.3	1.2	-21.1	2.5
[27]	CSRR, square	≈ 6.2	2.47	-28.4	1.56
Present work	CSRR, rectangular	≈ 10	5.15	-44.29	0.81

is the reference MUT having permittivity equal to 1 approximately. Hence, the parabolic equation (10) can further be expanded with respect to the permittivity of the reference MUT as

$$f_{r,\mathrm{MUT}} = A1 + A2(\varepsilon_{r,\mathrm{MUT}}\text{-}1) + A3(\varepsilon_{r,\mathrm{MUT}}\text{-}1)^2. \quad (11)$$

The constant parameters A_1, A_2, and A_3 are calculated by inserting the measured values of the standard MUTs (Air, Rogers 3003, and Quartz) from Table 3. After simplifications, the parabolic equation for the proposed sensor can be expressed as

$$f_{r,\mathrm{MUT}} = 5.07\text{-}0.378(\varepsilon_{r,\mathrm{MUT}}\text{-}1) + 0.029(\varepsilon_{r,\mathrm{MUT}}\text{-}1)^2. \quad (12)$$

The resonant frequency of the MUT ($f_{r,\mathrm{MUT}}$) can be estimated from the equation (12) by inserting the value of relative permittivity ($\varepsilon_{r,\mathrm{MUT}}$) of that material. The resonant frequencies of the standard MUTs, used in this work, are also calculated by inserting their values of real permittivity ($\varepsilon_{r,\mathrm{MUT}}$) in the equation (12). The calculated response is found very close to the measured response, which can be seen in Table 4. Error analysis is performed on the measured and calculated resonant frequencies. A very small percentage of error (% error) is achieved, as presented in Table 4, which indicates high accuracy of the proposed sensor.

The parabolic equation (12) is further simplified to estimate the relative permittivity ($\varepsilon_{r,\mathrm{MUT}}$) of any MUT, which can be expressed as

$$\varepsilon_{r,\mathrm{MUT}} = \frac{0.378\text{-}\sqrt{0.1428\text{-}0.116\left(5.07\text{-}f_{r,\mathrm{MUT}}\right)}}{0.058} + 1. \quad (13)$$

The relative permittivity ($\varepsilon_{r,\mathrm{MUT}}$) of any MUT can be approximated from the equation (13) by inserting the resonant frequency ($f_{r,\mathrm{MUT}}$) of the corresponding MUT. The relative permittivity of the standard MUTs used in this work is also calculated by inserting their measured resonant frequency ($f_{r,\mathrm{MUT}}$), mentioned in Table 3, in the equation (13). The calculated results of the relative permittivity of the MUTs are tabulated in Table 5. There is a negligible difference between the real and calculated permittivity of the MUTs. Error analysis is performed on the real and calculated permittivity of the MUTs. A very small percentage of error (% error) is obtained as shown in Table 5, which reveals high accuracy of the proposed sensor.

Performance of the proposed sensor is also analyzed by calculating the effective permittivity of a piece of wood and paper available in the lab. Both the materials are placed onto the sensor one by one and measuring the shift in the resonant frequency using the PNA-X. The measured responses of both the materials are illustrated in Figure 17 and also tabulated in Table 6.

The values of effective permittivity of both the MUTs are calculated using the parabolic equation (13) by inserting the measured resonant frequencies of both the MUTs one by one. The calculated values of the effective permittivity of both the MUTs are tabulated in Table 6. The calculated values of the permittivity of both the MUTs are found between the ranges of actual effective permittivity values provided in the data sheet, which show high accuracy of the proposed sensor.

3. Results and Discussions

The proposed sensor is used to measure the shift in the resonant frequency of the sensor due to the interaction with the MUTs and to approximate the relative permittivity of the corresponding MUTs using the formulated parabolic equation. In the present work, various standard materials including Rogers 5880, Rogers 3003, Plexi-glass, Quartz, and FR4 are used for the sensitivity analysis. The simulations and measurement are performed using the proposed sensor by placing these standard materials and measuring the shift in the resonant frequency of the sensor. The error bar graph with the standard deviation is presented, as shown in Figure 16, to showcase the performance of the proposed sensor in terms of the simulated and measured results. A strong agreement between the results and a very low standard deviation calculated from the measured results indicate high accuracy of the proposed sensor.

The resonant frequencies of the MUTs are also calculated using the formulated parabolic equation of the proposed sensor, which are tabulated in Table 4. The performance comparison among the simulated, measured, and calculated results in terms of the resonant frequency is carried out and illustrated graphically, as shown in Figure 18. The curves of all the results are in the strong agreement, which reveal high accuracy of the proposed sensor.

The sensor is proposed for the measurement of the relative permittivity of the MUTs. The relative permittivity of the standard MUTs is calculated using the formulated parabolic equation. The results of calculated permittivity of all the MUTs are found very close to the real permittivity of the corresponding MUT. Error analysis is performed between the real and calculated permittivity. A very small percentage of error is achieved. The performance comparison between the real and calculated permittivity is depicted graphically, as shown in Figure 19. Both the curves of the real and calculated permittivity are found very close, which shows a very strong agreement between them. A very small percentage of error and strong agreement between the results manifest the high accuracy of the proposed sensor.

A comparative analysis in terms of the overall performance is executed between the proposed sensor and the sensors reported in literature, which is shown in Table 7. A very small percentage of error "0.81%"" is achieved, which is the lowest as compared to the previous reported work. The accuracy of the proposed sensor is much better than that of the sensors reported in literature. Hence, the proposed sensor is highly accurate and efficient for the precise measurement of the dielectric properties of the materials under test.

4. Conclusions

A highly accurate complementary metamaterial sensor was proposed for the precise measurement of the relative permittivity of the materials under test. The proposed sensor was designed and simulated on Rogers' substrate RO4003C on using the ANSYS HFSS. The sensitivity of the proposed sensor was improved by introducing the slotted microstrip line on the top plane of the sensor. A single, sharp, and accumulative notch at -44.29 dB deep was achieved in the transmission coefficient (S_{21}) at the resonant frequency of 5.15 GHz by etching an array of four novel and compact resonators in the ground plane of the proposed sensor. The negative constitutive parameters (permittivity and permeability) were retrieved from the *S*-parameters which is the basic property of metamaterials or LHMs. The proposed sensor was fabricated and measured through the PNA-X (N5247A). The sensitivity analysis was performed by placing various standard materials onto the proposed sensor. A parabolic equation for the proposed sensor was formulated to approximate the relative permittivity of the materials under test. A very strong agreement was achieved among the simulated, measured, and calculated results of the proposed sensor. Error analysis is performed to determine the accuracy of the proposed sensor. A very small percentage of error "0.81%" and a very low standard deviation were achieved, which reveal high accuracy of the proposed sensor. The sensitivity analysis is carried out by placing various standard MUTs in solid format using the proposed sensor but the sensor can also be used effectively for the characterization of the MUTs in the powder format. The response of the proposed sensor is similar to the band-stop filter and hence can be used to design a narrow band-stop filter.

Data Availability

The data used to support the findings of this study are available from the corresponding author upon request.

Conflicts of Interest

The authors declare that there is no conflict of interest regarding the publication of this paper.

Acknowledgments

This research was funded by the National Natural Science Foundation of China having grant numbers [61527805], [61731001], and [41775030] and 111 Project of China having grant number [B14010].

References

[1] D. R. Smith, W. J. Padilla, D. C. Vier, S. C. Nemat-Nasser, and S. Schultz, "Composite medium with simultaneously negative permeability and permittivity," *Physical Review Letters*, vol. 84, no. 18, pp. 4184–4187, 2000.

[2] V. G. Veselago, "Reviews of topical problems: tThe electrodynamics of substances with simultaneously negative values of \epsilon and *M*," *Soviet Physics Uspekhi*, vol. 10, article R04, 1968.

[3] J. B. Pendry, A. J. Holden, D. J. Robbins, and W. J. Stewart, "Magnetism from conductors and enhanced nonlinear phenomena," *IEEE Transactions on Microwave Theory and Techniques*, vol. 47, no. 11, pp. 2075–2084, 1999.

[4] F. Falcone, T. Lopetegi, J. D. Baena, R. Marques, F. Martin, and M. Sorolla, "Effective negative-/Spl Epsiv/ stopband microstrip lines based on complementary split ring resonators," *IEEE Microwave and Wireless Components Letters*, vol. 14, no. 6, pp. 280–282, 2004.

[5] W. Fei, H. Yu, Y. Shang, D. Cai, and J. Ren, "A 96-Ghz oscillator by High-Q differential transmission line loaded with complementary split-ring resonator in 65-nm Cmos," *IEEE Transactions on Circuits and Systems II: Express Briefs*, vol. 60, no. 3, pp. 127–131, 2013.

[6] M. Abdolrazzaghi and M. Daneshmand, "A 4 Ghz near-field monitoring planar oscillator sensor," in *2018 IEEE MTT-S International Microwave Workshop Series on Advanced Materials and Processes for RF and THz Applications (IMWS-AMP)*, Ann Arbor, MI, USA, July 2018.

[7] L. Yang, W. Choi, K. Tam, and L. Zhu, "Novel wideband bandpass filter with dual notched bands using stub-loaded resonators," *IEEE Microwave and Wireless Components Letters*, vol. 27, no. 1, pp. 25–27, 2017.

[8] T. Haq, C. Ruan, X. Zhang, A. Kosar, and S. Ullah, "Low cost and compact wideband microwave notch filter based on miniaturized complementary metaresonator," *Applied Physics A*, vol. 125, no. 9, 2019.

[9] A. Ebrahimi, W. Withayachumnankul, S. Al-Sarawi, and D. Abbott, "High-sensitivity Metamaterial-inspired sensor for microfluidic dielectric characterization," *IEEE Sensors Journal*, vol. 14, no. 5, pp. 1345–1351, 2014.

[10] J. Mata-Contreras, C. Herrojo, and F. Martín, "Application of split ring resonator (Srr) loaded transmission lines to the design of angular displacement and velocity sensors for space applications," *IEEE Transactions on Microwave Theory and Techniques*, vol. 65, no. 11, pp. 4450–4460, 2017.

[11] A. Ebrahimi, W. Withayachumnankul, S. F. Al-Sarawi, and D. Abbott, "Metamaterial-inspired rotation sensor with wide dynamic range," *IEEE Sensors Journal*, vol. 14, no. 8, pp. 2609–2614, 2014.

[12] M. Abdolrazzaghi, M. Daneshmand, and A. K. Iyer, "Strongly enhanced sensitivity in planar microwave sensors based on Metamaterial coupling," *IEEE Transactions on Microwave Theory and Techniques*, vol. 66, no. 4, pp. 1843–1855, 2018.

[13] A. T. Devapriya, G. Rani, and S. Robinson, "Dual resonant microstrip patch antenna using metamaterial planar structures for S band and C band applications," *ICTACT Journal on Communication Technology*, vol. 7, no. 4, 2016.

[14] J. Xu, L. Tao, R. Zhang, Y. Hao, S. Huang, and K. Bi, "Broadband complementary ring-resonator based terahertz antenna," *Optics Express*, vol. 25, no. 15, pp. 17099–17104, 2017.

[15] Y. D. Sirmaci, C. K. Akin, and C. Sabah, "Fishnet based metamaterial loaded Thz patch antenna," *Optical and Quantum Electronics*, vol. 48, no. 2, 2016.

[16] R. A. Alahnomi, Z. Zakaria, E. Ruslan, A. A. Mohd Bahar, and S. R. Ab Rashid, "High sensitive microwave sensor based onsymmetrical split ring resonator for material characterization," *Microwave and Optical Technology Letters*, vol. 58, no. 9, pp. 2106–2110, 2016.

[17] J. D. Baena, J. Bonache, F. Martin et al., "Equivalent-circuit models for split-ring resonators and complementary split-ring resonators coupled to planar transmission lines," *IEEE Transactions on Microwave Theory and Techniques*, vol. 53, no. 4, pp. 1451–1461, 2005.

[18] R. A. Alahnomi, Z. Zakaria, E. Ruslan, S. R. Ab Rashid, and A. A. Mohd Bahar, "High-Q sensor based on symmetrical split ring resonator with spurlines for solids material detection," *IEEE Sensors Journal*, vol. 17, no. 9, pp. 2766–2775, 2017.

[19] J. Dong, F. Shen, Y. Dong et al., "Noncontact measurement of complex permittivity of electrically small samples at microwave frequencies," *IEEE Transactions on Microwave Theory and Techniques*, vol. 64, no. 9, pp. 2883–2893, 2016.

[20] A. Bahar, A. Mohd, Z. Zakaria, S. R. Ab Rashid, A. A. M. Isa, and R. A. Alahnomi, "High-efficiency microwave planar resonator sensor based on bridge split ring topology," *IEEE Microwave and Wireless Components Letters*, vol. 27, no. 6, pp. 545–547, 2017.

[21] A. Ebrahimi, J. Scott, and K. Ghorbani, "Differential sensors using microstrip lines loaded with two split-ring resonators," *IEEE Sensors Journal*, vol. 18, no. 14, pp. 5786–5793, 2018.

[22] M. A. H. Ansari, A. K. Jha, and M. J. Akhtar, "Design and application of the Csrr-based planar sensor for noninvasive measurement of complex permittivity," *IEEE Sensors Journal*, vol. 15, no. 12, pp. 7181–7189, 2015.

[23] C. Yang, C. Lee, K. Chen, and K. Chen, "Noncontact measurement of complex permittivity and thickness by using planar resonators," *IEEE Transactions on Microwave Theory and Techniques*, vol. 64, no. 1, pp. 247–257, 2016.

[24] A. M. Albishi and O. M. Ramahi, "Surface crack detection in metallic materials using sensitive microwave-based sensors," in *2016 IEEE 17th Annual Wireless and Microwave Technology Conference (WAMICON)*, Clearwater, FL, USA, April 2016.

[25] L. Su, J. Mata-Contreras, P. Velez, A. Fernandez-Prieto, and F. Martin, "Analytical method to estimate the complex permittivity of oil samples," *Sensors*, vol. 18, no. 4, p. 984, 2018.

[26] X. Zhang, C. Ruan, T. U. Haq, and K. Chen, "High-sensitivity microwave sensor for liquid characterization using a complementary circular spiral resonator," *Sensors*, vol. 19, no. 4, 2019.

[27] M. Saadat-Safa, V. Nayyeri, M. Khanjarian, M. Soleimani, and O. M. Ramahi, "Full characterization of magneto-dielectric materials using a novel Csrr based sensor," in *2018 9th International Symposium on Telecommunications (IST)*, Tehran, Iran, December 2018.

[28] C. Lee and C. Yang, "Thickness and permittivity measurement in multi-layered dielectric structures using complementary split-ring resonators," *IEEE Sensors Journal*, vol. 14, no. 3, pp. 695–700, 2014.

[29] C.-S. Lee and C.-L. Yang, "Complementary split-ring resonators for measuring dielectric constants and loss tangents," *IEEE Microwave and Wireless Components Letters*, vol. 24, no. 8, pp. 563–565, 2014.

[30] R. Kumari, P. N. Patel, and R. Yadav, "An eng-inspired microwave sensor and functional technique for label-free detection of *Aspergillus Niger*," *IEEE Sensors Journal*, vol. 18, no. 10, pp. 3932–3939, 2018.

[31] S. Trabelsi and S. O. Nelson, "Microwave sensing of quality attributes of agricultural and food products," *IEEE Instrumentation & Measurement Magazine*, vol. 19, no. 1, pp. 36–41, 2016.

[32] M. Puentes, M. Maasch, M. Schubler, and R. Jakoby, "Frequency multiplexed 2-dimensional sensor array based on split-ring resonators for organic tissue analysis," *IEEE Transactions on Microwave Theory and Techniques*, vol. 60, no. 6, pp. 1720–1727, 2012.

[33] M. Abdolrazzaghi, S. Khan, and M. Daneshmand, "A dual-mode split-ring resonator to eliminate relative humidity impact," *IEEE Microwave and Wireless Components Letters*, vol. 28, no. 10, pp. 939–941, 2018.

[34] K. Technologies, *Basics of Measuring the Dielectric Properties of Materials*, © Keysight Technologies, USA, 5989-2589EN, 2018.

[35] A. Vivek, K. Shambavi, and C. Alex Zachariah, "A review: metamaterial sensors for material characterization," *Sensor Review*, vol. 39, no. 3, pp. 417–432, 2019.

[36] M. A. H. Ansari, A. K. Jha, and M. J. Akhtar, "Dual band microwave sensor for dielectric characterization of dispersive materials," in *2015 Asia-Pacific Microwave Conference (APMC)*, Nanjing, China, Decemeber 2015.

[37] T. U. Haq, C. Ruan, R. Wang, and T. Wu, "High Q dual band super high frequency notch Filter based on complementary metamaterial," in *2018 Progress in Electromagnetics Research Symposium (PIERS-Toyama)*, Toyama, Japan, August 2018.

[38] M. A. H. Ansari, A. K. Jha, Z. Akhter, and M. J. Akhtar, "Multi-band Rf planar sensor using complementary split ring resonator for testing of dielectric materials," *IEEE Sensors Journal*, vol. 18, no. 16, pp. 6596–6606, 2018.

[39] L. Su, J. Naqui, J. Mata-Contreras, and F. Martín, "Modeling and applications of Metamaterial transmission lines loaded with pairs of coupled complementary split-ring resonators

(Csrrs)," *IEEE Antennas and Wireless Propagation Letters*, vol. 15, pp. 154–157, 2016.

[40] J.-S. Hong, *Microstrip Filters for Rf/Microwave Applications. Second ed*, A John Wiley & Sons, Inc., Hoboken, NJ, USA, 2011.

[41] M. S. Boybay and O. M. Ramahi, "Material characterization using complementary split-ring resonators," *IEEE Transactions on Instrumentation and Measurement*, vol. 61, no. 11, pp. 3039–3046, 2012.

[42] X. Chen, T. M. Grzegorczyk, B. I. Wu, J. Pacheco Jr., and J. A. Kong, "Robust method to retrieve the constitutive effective parameters of metamaterials," *Physical Review. E, Statistical, Nonlinear, and Soft Matter Physics*, vol. 70, no. 1, article 016608, 2004.

[43] S. Lim, C. Kim, and S. Hong, "Simultaneous measurement of thickness and permittivity by means of the resonant frequency fitting of a microstrip line ring resonator," *IEEE Microwave and Wireless Components Letters*, vol. 28, no. 6, pp. 539–541, 2018.

[44] M. S. K T, M. A. H. Ansari, A. K. Jha, and M. J. Akhtar, "Design of Srr-based microwave sensor for characterization of magnetodielectric substrates," *IEEE Microwave and Wireless Components Letters*, vol. 27, no. 5, pp. 524–526, 2017.

[45] K. Shafi, T. Muhammed, A. K. Jha, and M. J. Akhtar, "Improved planar resonant Rf sensor for retrieval of permittivity and permeability of materials," *IEEE Sensors Journal*, vol. 17, no. 17, pp. 5479–5486, 2017.